Chemical Methodologies

Journal homepage: http://chemmethod.com

Original Research article

Removal of Methylene Blue from Aqueous Solutions using Nano-Magnetic Adsorbent Based on Zinc-Doped Cobalt Ferrite

Ibrahim A. Amar[a, b] *, Abubaker Sharif[c], Manal Ali[a], Sharefa Alshareef[a], Fatima Altohami[a], Mabroukah A. AbdulQadir[a], Mohammed M. Ahwidi[a]

[a] Department of Chemistry, Faculty of Science, Sebha University, Sebha, Libya

[b] Central Laboratory at Sebha University, Sebha, Libya

[c] Advanced Laboratory of Chemical Analysis, Authority of Natural Science Research and Technology, Tripoli, Libya

ARTICLE INFORMATION

Received: 18 March 2019
Received in revised: 26 April 2019
Accepted: 07 June 2019
Available online: 18 August 2019

DOI: 10.33945/SAMI/CHEMM.2020.1.1

KEYWORDS

Spinel ferrite nanoparticles
Adsorption
Dye removal
Kinetics
Isotherms
Thermodynamics

ABSTRACT

In this study, Zn-substituted cobalt ferrite nanoparticles ($CoFe_{1.9}Zn_{0.1}O_4$, CFZ) were successfully synthesized *via* a combined EDTA-citrate sol-gel process. The synthesized $CoFe_{1.9}Zn_{0.1}O_4$ nanoparticles were characterized by X-ray powder diffraction (XRD), Fourier transform infrared spectroscopy (FTIR), point zero charge (pH_{pzc}) and scanning electron microscopy (SEM). The adsorption experiments of methylene blue (MB) onto CFZ surface were conducted in batch mode. The experiments were conducted under different conditions (contact time, adsorbent dosage, initial pH solution, solution temperature and initial dye concentration). The experimental data were better fitted to pseudo-second-order (PSO) kinetic model (R^2=0.9990). In addition, Langmuir isotherm (R^2=0.9906) was the best model to describe the experimental adsorption data. The maximum adsorbed amount of MB (q_{max}) per unit mass of adsorbent was about 27.79 mg/g. The adsorption thermodynamics (*i.e.*, $\Delta G°$, $\Delta H°$, $\Delta S°$) revealed that the proposed adsorption process is feasible, spontaneous and exothermic in nature. The obtained results suggest that CFZ is a promising material used as an adsorbent for very toxic pollutants from aqueous solutions.

*Corresponding author: E-mail: ibr.amar@sebhau.edu.ly, Department of Chemistry, Faculty of Science, Sebha University, Sebha, Libya, Central Laboratory at Sebha University, Sebha, Libya, Tel: Tel: +218-94-5173068; Fax: +218-71-2627039

Graphical Abstract

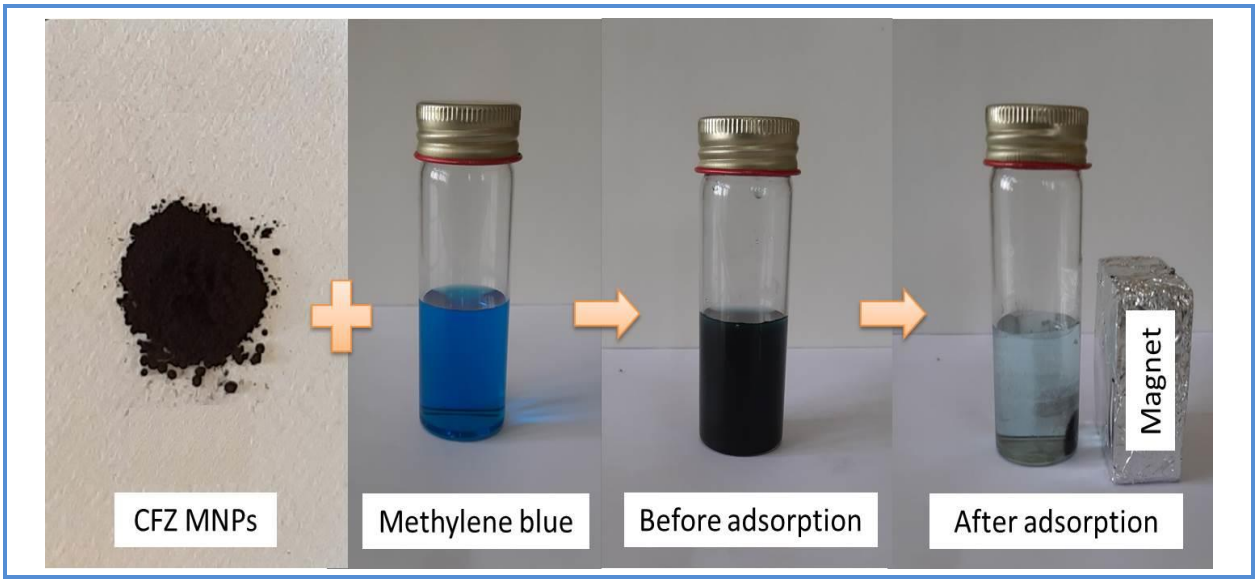

Introduction

Synthetic dyes of different kinds are commonly used in various processing steps by many industries; including textile, plastics, cosmetics, paper, food, and leather *etc.* [1-3]. Most of these organic dyes are mutagenic, carcinogenic and toxic [4, 5]. Therefore, discharging of such dyestuffs into water systems is considered as the most worldwide environmental problem [6]. In general, cationic dyes are very toxic in comparison to anionic dyes [7]. Methylene blue (MB) which is extensively used as a colourant agent for cotton, wool and silk is a typical example of these dyes [1]. However, the exposure to MB may cause nausea, vomiting, jaundice, increased heart rate, profuse sweating, mental confusion, cyanosis and quadriplegia, *etc.* [1, 2]. Thus, it is of crucial importance to treat dye-contaminated water before being released into the aquatic environment.

Up to now, different techniques including membrane filtration, coagulation-flocculation, photocatalytic degradation, chemical oxidation and adsorption, *etc.* [2-8] have been developed for removing very toxic organic dyes from aqueous solutions. Among these methods, adsorption is superior owing to its unique properties including ease of operation, low operational cost, simplicity of design, insensitivity to toxic pollutants, high removal efficiency and availability of various adsorbent types, *etc.* [2, 5, 9-11].

Activated carbon (AC) is widely used as adsorbent material for treating dye-contaminated water owing to its large surface area, porous structure and good adsorption performance, *etc.* However, the high production cost, sludge formation, disposal, recovery and regeneration are still remaining

the drawbacks that limit the applications of AC in water treatment technologies [2-9]. In addition, the separation of AC using the conventional filtration method usually results in the loss of AC and blockage of the filter [12].

Magnetic separation technique was developed with the aim of overcoming the aforementioned problems associated with the conventional filtration method. In this technique, the adsorbent should possess adequate magnetic properties to be easily separated from the adsorption medium using an external magnetic field [12-14].

In recent years, magnetic nanoparticles (MNPs) are considered as alternative adsorbent materials for the development of water treatment technologies [15, 16]. Among MNPs, spinel ferrites (SFs) have attracted more attention owing to their diverse structures, fast adsorption kinetics, high specific surface area, moderate saturation magnetization, ease of functionalization, easy of separation from adsorption medium with the aid of an external magnetic field, ease of recovery and regeneration, chemical and thermal stabilities, *etc.* [5, 15-17]. Thus, different spinel ferrite nanoparticles (SFNPs) and their nanocomposites (SFNCs) were tested as adsorbents for the removal MB dye from aqueous solutions. These include; $MnFe_2O_4$ [18], $NiFe_2O_4$ [19], $CoFe_{1.9}Mo_{0.1}O_4$ [20], polyaniline/$NiFe_2O_4$ [21] and activated carbon/$Mn_{0.6}Zn_{0.4}Fe_2O_4$ [22]. Despite that fact that many SFNPs and SFNCs were employed as adsorbent materials for removing MB from aqueous solutions, no report was found in the literature on using Zn-substituted cobalt ferrite magnetic nanoparticles ($CoFe_{1.9}Zn_{0.1}O_4$) for treating aqueous environments containing such a toxic dye. Therefore, the main aim of the present work is to investigate the adsorption characterises of $CoFe_{1.9}Zn_{0.1}O_4$ MNPs for removing MB dye from aqueous solution.

Experimental

Materials

In this study, all chemicals (Table 1) were used as received.

Table 1. List of the used chemical compounds

Material	Formula	Supplier
Zinc nitrate hexahydrate	$Zn(NO_3)_2{\cdot}6H_2O$	T. Baker Lab Chemicals
Iron nitrate nonahydrate	$Fe(NO_3)_3{\cdot}9H_2O$	Berck and Scientific Supplies
Cobalt nitrate hexahydrate	$Co(NO_3)2{\cdot}6H_2O$	Analyticals
Sodium hydroxide	NaCl	Fluka
Ammonia solution (35%)	NH_3	Scharlau
Citric acid	$C_6H_8O_7$	Labkem
Ethylenediaminetetraacetic acid[a]	$C_{10}H_{18}N_2O_8$	Serva
Hydrochloric acid	HCl	BDH Chemicals
Methylene blue dye	$C_{16}H_{18}ClN_3S{\cdot}xH_2O$, x = 2-3	Surechem Products (ScP)

[a] EDTA

Synthesis of $CoFe_{1.9}Zn_{0.1}O_4$ nanoparticles

$CoFe_{1.9}Zn_{0.1}O_4$ nanoparticles (CFZ NPs) were synthesized *via* a combined EDTA-citrate complexing sol-gel process [23]. Firstly, the required amounts of $Fe(NO_3)_3{\cdot}9H_2O$, $Co(NO_3)_2{\cdot}6H_2O$ and $Zn(NO_3)_2{\cdot}6H_2O$ were dissolved in deionized water. Then, citric acid and EDTA were added as complexing agents at molar ratio of citric acid: EDTA: metal cations of 1.5: 1: 1. Then, a diluted ammonia solution was added to adjust the pH value of the mixed solution to~6. The mixture was stirred under heating on a hot-plate until a black sticky gel was formed. The gel precursor was further heated to dryness before being converted to a solid product (ash). Finally, the ash was calcined in air at 600 °C for 3 h to get $CoFe_{1.9}Zn_{0.1}O_4$ magnetic nanoparticles.

Characterization of $CoFe_{1.9}Zn_{0.1}O_4$ nanoparticles

The crystal structure and phase purity of $CoFe_{1.9}Zn_{0.1}O_4$ NPs were characterized by X-ray powder diffraction (XRD) technique using a Philips–PW 1800 diffractometer with CuKα radiation (λ=1.54186 Å). The crystallite size (D), lattice parameters (α), unit cell volume (V_{cell}), the X-ray density (ρ_{XDR}) and the specific surface area (S_{XRD}) of $CoFe_{1.9}Zn_{0.1}O_4$ NPs were estimated using the following Equations [3, 24];

$$D = \frac{0.9\,\lambda}{(\beta\cos\theta)} \tag{1}$$

$$a = d_{hkl}\sqrt{h^2 + k^2 + l^2} \tag{2}$$

$$V_{cell} = a^3 \tag{3}$$

$$\rho_{XRD} = \frac{ZM}{N_A V_{cell}} \tag{4}$$

$$S_{XRD} = \frac{6000}{D \cdot \rho_{XRD}} \tag{5}$$

Where λ is the wavelength of the X-ray, θ is the Bragg angle, β is the full width at half maximum (FWHM) of the peak in radiance, d is the interplanar distance, hkl are the Miller indices, M is the molecular weight of the sample, Z is the number of molecules per formula unit (Z=8 for spinel system) and N_A is the Avogadro's number.

Fourier transform infrared (FTIR) spectrum of CFZ NPs was recorded with the help of Bruker tensor 27 spectrophotometer using a KBr disc method in the range of 400-4000 cm^{-1}. Scanning electron microscope (SEM) was used to investigate the surface morphology of the prepared CFZ

NPs using a LEO 1430PV instrument. The pH at the point of zero charge (pH_{PZC}) of CFZ NPs was estimated using the typical "drift method", as described elsewhere [25]. In brief, 0.1 g of CFZ NPs were transferred into series flasks containing a 25 mL of NaCl solution (0.1 mol/L) with different initial pH values (pH_i = 3, 5, 7, 9, 11). The flasks were closed tightly before being shaken for 24 h, then the final pH value (pH_f) was measured. Finally, the pH_{PZC} value was estimated by plotting the ΔpH (pH_i -pH_f) against the pH_i [26]. It is to be noted that the pH_i of NaCl solution was adjusted using either a 0.1 mol/L solution of HCl or NaOH and all pH_{PZC} experiments were carried out at room temperature (~ 25 °C).

Adsorption studies

Adsorption experiments

Batch adsorption experiments were designed to investigate the adsorption properties of CFZ nanoparticles for methylene blue (MB) dye. A stock solution of MB (100 mg/L) was prepared by dissolving the required amount of MB into deionized water. The desired concentration of MB was obtained by further diluting the stock solution of the dye using deionized water. The adsorption experiments were carried out in series of 25 mL Erlenmeyer flasks that contain 20 mL of MB solution and certain amount of the adsorbent material (CFZ). The flasks were tightly closed, placed on an orbital shaker (IKA-Werke) then shaken for specific time at the speed of 320 rpm [20]. Different experimental conditions were studied including; initial solution pH (3-11), contact time (0-120 min), initial MB concentration (10-90 mg/L), adsorbent dosage (0.01-0.09 g/20 mL) and solution temperature (25-45 °C). The initial pH value of MB dye solution was adjusted using a diluted solution of either (0.1 mol/L) HCl or NaOH. The concentration of MB before and after the adsorption experiment was measured using a single beam UV-vis spectrophotometer (Jenway model 6305) at a maximum wavelength λ_{max} of 662 nm [1]. After the adsorption experiments, the CFZ magnetic nanoparticles could be separated easily using an external magnet. The percentage of MB removal ($\%R$), the amount of MB adsorbed per unit mass of adsorbent at any time t (q_t, mg/g) and at equilibrium (q_e, mg/g), are calculated using the following equations [4, 27];

$$\%R = \frac{C_o - C_t}{C_o} \times 100 \quad (6)$$

$$q_t = \frac{V(C_o - C_t)}{m} \quad (7)$$

$$q_e = \frac{V(C_o - C_e)}{m} \quad (8)$$

Where, C_o, C_t, C_e (mg/L) are initial dye concentration, final dye concentration at any time t and dye concertation at the equilibrium, respectively. V (L) is the volume of dye solution and m (g) is the adsorbent dosage. The adsorption experiments were triplicated and the mean value ± standard error (SE) was used to express the experimental data.

Adsorption kinetic models

In this study, the adsorption kinetics were described by fitting the experimental data to pseudo-first-order (PFO) [28] and pseudo-second-order (PSO) kinetic models [29]. The linearized forms of PFO and PSO can be expressed as described below [30];

$$\ln(q_e - q_t) = \ln q_e - k_1 t \tag{9}$$

$$\frac{t}{q_t} = \frac{1}{k_2 q_e^2} + \frac{1}{q_e} t \tag{10}$$

Where, k_1 (min^{-1}) and k_2 (g/mg min) are constants related to PFO and PSO kinetic models. The value of q_e was derived from the intercept and the value of k_1 was calculated from slope of the plot of $\ln(q_e - q_t)$ versus t.

Isotherm models

To better understand the nature adsorbate/adsorbent interaction, the adsorption experimental data were fitted using Langmuir [31] and Freundlich [32] isotherm models. Langmuir is the most suitable isotherm model to describe the adsorption on homogenous surfaces, whereas the adsorption on heterogeneous surfaces can be better described using Freundlich isotherm model. Langmuir and Freundlich isotherms can be expressed in the linearized forms using Equations (11) and (12), respectively [30];

$$\frac{C_e}{q_e} = \frac{1}{q_{max} K_L} + \frac{1}{q_{max}} \tag{11}$$

$$\ln q_e = \ln K_F + \frac{1}{n} \ln C_e \tag{12}$$

where q_{max} (mg/g) is the maximum adsorbed amount of MB, K_L (L/mg) and K_F ((mg/g)/(mg/L)^n) are constants related to Langmuir and Freundlich isotherm models, respectively. n (dimensionless) is Freundlich intensity parameter, which indicates the degree of adsorbent surface heterogeneity and the adsorption process favourability. The adsorption is linear n=1, favourable (n<1), unfavourable (n>1) and irreversible n=0. In addition, the slope $(1/q_{max})$ and the intercept $(1/q_{max} K_L)$ of the linear plot of C_e against (C_e/q_{max}) were used to estimate the values of q_{max} and K_L respectively. The values of

K_F and n, were calculated from the intercept ($\ln K_F$) and the slope ($1/n$) of the linear plot of $\ln C_e$ against $\ln q_e$. Equation (13) expresses a dimensionless constant called separation factor (R_L) which related to Langmuir isotherm model.

$$R_L = \frac{1}{1 + K_L C_e} \quad (13)$$

The R_L value can be used to evaluate the adsorption process feasibility. The adsorption characteristics can be described by the R_L value as follows; favourable ($0<R_L<1$), linear ($R_L > 1$), unfavourable ($R_L>1$) and irreversible ($R_L = 0$) [30].

Adsorption thermodynamics

The adsorption thermodynamics were interpreted using Gibb's free energy change (ΔG^o, kJ/mol), enthalpy change (ΔH^o, kJ/mol) and entropy change (ΔS^o, kJ/mol.K). The values of the thermodynamic parameters were estimated using the following equations [30, 33];

$$\Delta G^o = \Delta H^o - T\Delta S^o \quad (14)$$

$$\ln K_c = \frac{-\Delta H^o}{R}\frac{1}{T} + \frac{\Delta S^o}{R} \quad (15)$$

$$K_c = \frac{C_s}{C_e} \quad (16)$$

Where, K_c is the thermodynamic constant (dimensionless) known also as distribution coefficient. The value of K_c can be estimated using Equation (15). C_s is the concentration of MB (mg/L) on the adsorbent surface. T is absolute temperature (K) and R is the universal gas constant (8.314 J/mol/K). In addition, by plotting $\ln K_c$ versus $(1/T)$, the values of ΔH^o (slope) and ΔS^o (intercept) can be determined.

Results and discussion

Characterization of $CoFe_{1.9}Zn_{0.1}O_4$ adsorbent

In this study, different techniques (XRD, FTIR, SEM and pH_{PZC}) were used to characterize the prepared CFZ magnetic nanoparticles (Figure 1). The XRD pattern of CFZ NPs is shown in Figure 1a. As shown, a single phase of CFZ NPs is obtained after firing its corresponding ash in air at 600 °C for 3 h. Furthermore, no extra peaks were noticed and all diffraction peaks observed in XRD pattern are well indexed to those reflections typically found in the cubic structure of magnetite (JCPDS card No. 19-0629). In addition, the crystallite size (D=35.39 nm), lattice parameters (a=b=c=8.2707 Å), unit cell

volume (V_{cell}=565.75 Å^3), the X-ray density (ρ_{XDR}=5.53 g/cm^3) and the specific surface area (S_{XRD}=30.66 m^2/g) of $CoFe_{1.9}Zn_{0.1}O_4$ NPs were estimated using XRD date of the most intense reflection (311).

The FTIR spectrum of CFZ magnetic nanoparticles within the wavenumber range of 400 to 4000 cm^{-1} is shown in Figure 1b. In the spectrum, the absorption peaks at 446 and 527 cm^{-1} could be ascribed to stretching vibration of metal-oxygen bonds (Fe-O) at octahedral and tetrahedral sites, respectively. These two peaks suggest the formation of spinel ferrite-type oxides [34]. The absorption peaks from 716 to 1068 cm^{-1} are assigned to the vibration of NO_3^- group [27]. The observed peak at 1436 cm^{-1} could be attributed to C-H bending vibration [35]. In addition, the broad absorption band at 3433 cm^{-1} could be assigned to stretching vibration of O-H [27].

Scanning electron microscopy (SEM) was used to investigate the surface morphology of the CFZ nanoparticles, as shown in Figure 1c. As can be seen from the SEM image, the surface of CFZ NPs consists of large grains which are surrounded by small particles. It can be also seen from the SEM image the porous structure of the prepared CFZ magnetic nanoparticles. These pores are believed to play an important role in adsorption process. Figure 1d represents the pH_{PZC} of the prepared magnetic nanoparticles (CFZ). As shown, the estimated pH_{PZC} value was found to be 6.53.

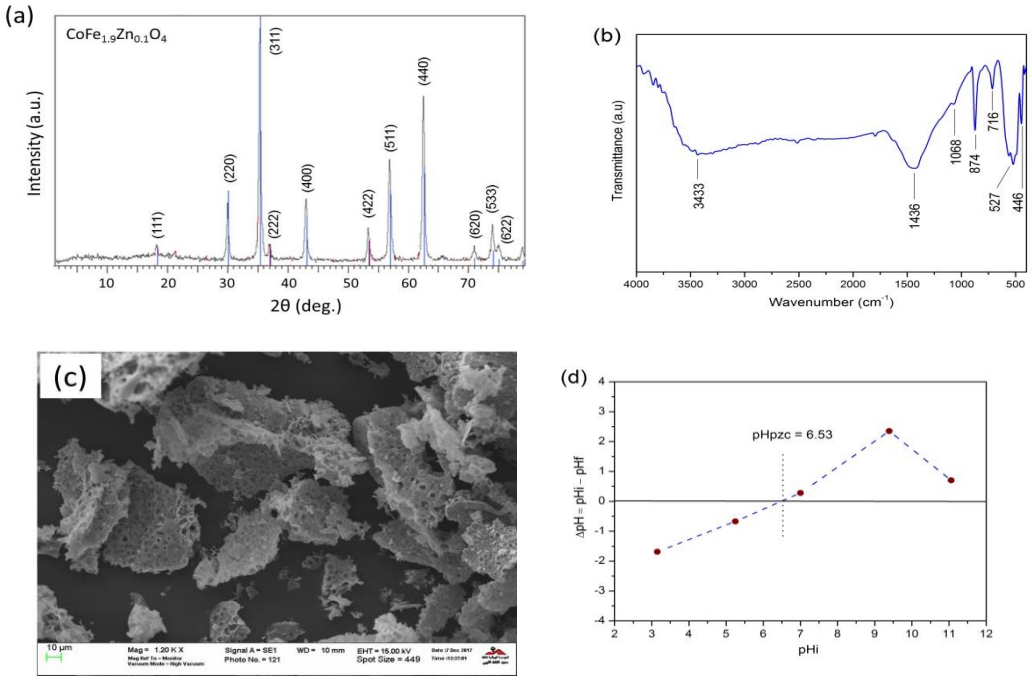

Figure 1. (a) X-ray diffraction pattern; (b) FTIR spectrum; (c) SEM image; (d); pH at the point of zero charge of $CoFe_{1.9}Zn_{0.1}O_4$ magnetic nanoparticles

Effect of operational parameters on dye adsorption

Effect of solution pH

In order to investigate the effect of MB dye solution pH on the removal percentage (%R) of MB, the initial pH value was varied from 3 to 11. The experiment was performed at fixed amount of adsorbent (0.01 g/20 mL), initial dye concentration of 100 mg/L and under a contact time of 60 min. Figure 2 shows the effect of initial solution pH on the removal percentage of MB using CFZ as adsorbent. As can be seen, increasing the initial solution pH from 3 to 7 resulted in increasing the %R value of MB. However, when the pH was further increased above 7, the %R value of MB decreased. Hence, an initial pH value of 7 was selected for the subsequent experiments. To understand this behaviour (*i.e.,* pH dependence), the characteristics of both CFZ nanoparticles and MB dye should be taken into consideration. As mentioned earlier, the pH_{PZC} of the CFZ nanoparticles was about 6.53 (Figure 1d). This means that, the charge of CFZ surface will be positive at solution pH value lower than 6.53 ($pH<pH_{pzc}$) and negative at pH value higher than it ($pH>pH_{pzc}$) [15]. In addition, in aqueous solutions, MB (cationic dye) will give positively charged ions [36]. Thus, the observed low %R value of MB at low solution pH (pH<6.53) could be as a result of the electrostatic repulsion between CFZ NPs surface (positively charged) and MB dye molecules (positive ions). Moreover, the high observed %R value of MB at initial solution pH of 7 might be due to the electrostatic attraction between the negatively charged surface of CFZ NPs and of MB molecules (positively charged ions). However, the decrease in the %R value at pH value higher than 7 despite that fact that MB ions and CFZ surface are differently charged, might be due to the increase in the ionic strength of dye solution as a result of the formation NaCl. As reported previously by *Al-Anber* et al., [37], NaCl is formed because of the replacement reaction between MB which contains Cl^- (Table 1) and NaOH that used for adjusting the initial value of dye solution.

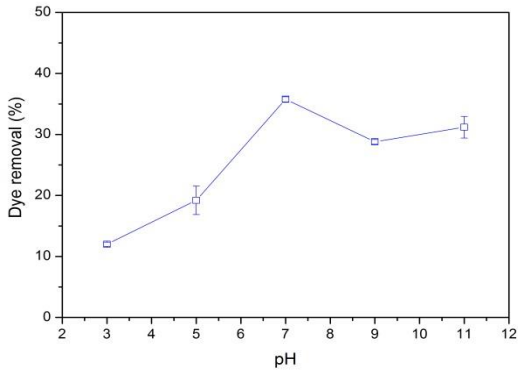

Figure 2. Effect of initial pH on the MB removal percentage

Effect of contact time

Figure 3 shows the effect of contact time on the removal percentage of MB (%R). In this experiment, the contact time was changed and the other experimental conditions were kept at the optimized values (initial pH of 7 and adsorbent dosage of 0.01 g/20 mL). As shown, an increase in the %R value was observed by increasing the contact time and a value of about 34 % was attained when the contact reached 20 min. However, by further increasing the contact time, the %R was increased slightly reaching a maximum value of about 37at a contact time of 90 min. Thus, the subsequent adsorption experiments were performed at 90 min. This insignificant increase in the %R value with contact time could be due to the fact that all active binding sites on adsorbent surface (CFZ) became saturated after the adsorption certain amount of MB molecules [4].

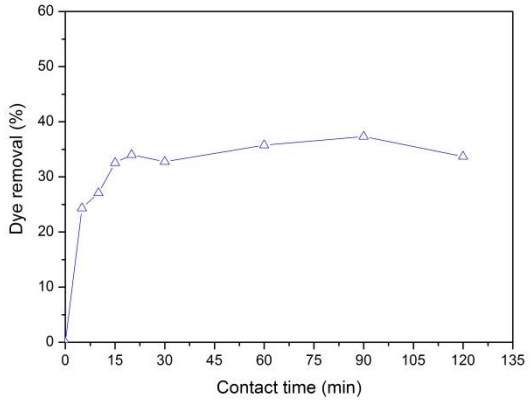

Figure 3. Effect of contact on the MB removal percentage

Effect of the initial dye concentration

To evaluate the effect of initial dye concentration on the %R of MB, the adsorption experiments were conducted at various initial MB concentrations (10 to 90 mg/L) and under the optimized values of the other experimental conditions (adsorbent dosage of 0.01 g/20 mL, initial pH of 7 and contact time of 90 min). The obtained results are demonstrated in Figure 4. It is clearly seen from the figure that the %R of MB decreased significantly from 76.78% to 15.57% with as the initial MB concentration was increased from 10 to 90 mg/L, respectively. This behaviour could be due to the fact that, after the adsorption of a certain amount of MB, the available number of active sites on the CFZ surface became saturated [38]. Based on this finding, an initial MB concentration of 10 mg/L was chosen as optimum value and will be used in the subsequent experiments.

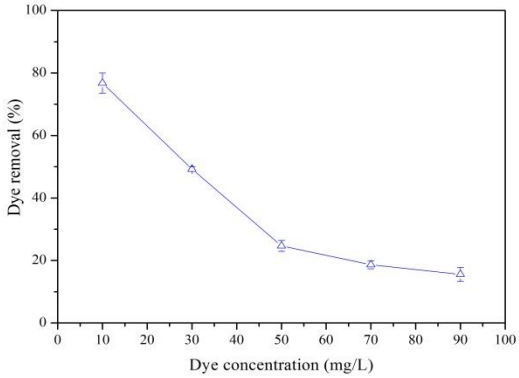

Figure 4. Effect of the initial dye concentration on the MB removal percentage

Effect of adsorbent dosage

The effect of the amount of the adsorbent (CFZ NPs) on the %R value and the adsorbed amount of MB at the equilibrium (q_e, mg/g) was investigated by varying the adsorbent dosage from 0.01 to 0.09 g/20 mL. Besides, the other experimental conditions were fixed at constant values (solution pH of 7, contact time of 90 min and MB concentration of 10 mg/L). The obtained results are shown in Figure 5. As seen from the figure, the R% and q_e values of MB decreased as the mount of CFZ NPs was increased from 0.01 to 0.03 g/20 mL. This could be due to the reduction in the total surface area of the adsorbent surface (CFZ NPs) as a result of overlapping or aggregation of the available active sites on the adsorbent surface with increasing the adsorbent dosage [1]. However, when the adsorbent dosage was further increased the %R and q_e of MB remained almost at constant values. Thus, a mass of 0.01 g/20 mL was selected as an optimum adsorbent dosage at which the %R and q_e of MB values were about 76.78% and 15.36 mg/g, respectively.

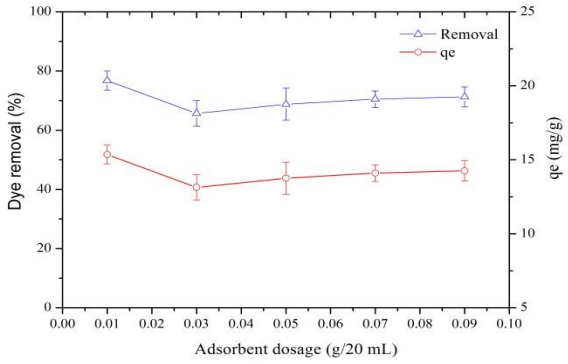

Figure 5. Effect of the adsorbent dosage on the MB removal percentage and the amount of MB adsorbed at the equilibrium

Effect of solution temperature

At the present study, three different solution temperatures (25, 35 and 45 °C) were selected to investigate their effect on the adsorption behaviour of MB onto CFZ NPs. Besides, the other adsorption experimental conditions were fixed at the optimized values (pH value of 7, initial MB concentrations of 10 mg/L, adsorbent dosage of 0.01 g/20 mL and contact time of 90 min). As can be seen from Figure 6, as the dye solution temperature increased, the %R value of MB was decreased. This phenomenon indicates the exothermic in nature of the proposed adsorption process [10]. In addition, the decrease in the %R value is due to the weaker bonds between the adsorbent sites and MB molecules as result of increasing solution temperature [39].

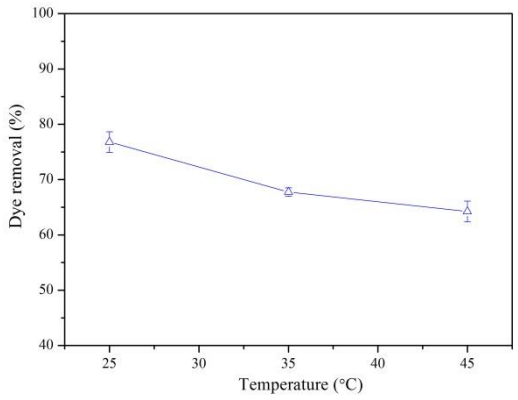

Figure 6. Effect of solution temperature on the MB removal percentage

Adsorption kinetics

In this study, the experimental adsorption data were fit using pseudo-first-order (PFO) and pseudo-second-order (PSO) kinetic models, as shown in Figure 7. The kinetic models (PFO and PSO) fitting parameters are listed in Table 2. The goodness of fit between the calculated ($q_{e,cal}$) and the experimental data ($q_{e,exp}$) was determined using correlation coefficient (R^2). As shown from Table 2, PSO kinetic model exhibit higher R^2 value (0.9990) compared to that of PFO model (0.5195). In addition, the value of $q_{e,exp}$ obtained from PSO was consistent with $q_{e,cal}$ value. This indicates that the adsorption of MB onto CFZ NPs obeys the PSO kinetic model.

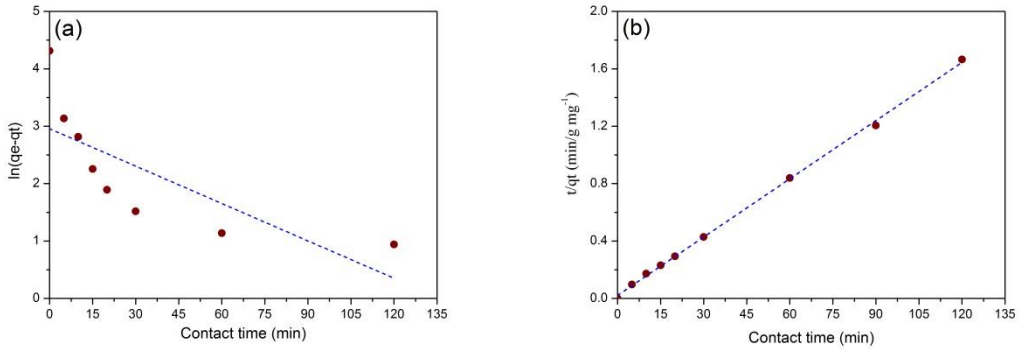

Figure 7. Adsorption kinetics for removal of MB on CFZ: (a) pseudo-first-order and (b) pseudo-second order models

Table 2. Kinetic parameters for the adsorption of MB onto CFZ nanoparticles

$q_{e,exp}$ (mg/g)	Pseudo-first-order		
	$q_{e,cal}$ (mg/g)	k_1 (min^{-1})	R^2
74.64	19.23	2.17×10^{-2}	0.5195
	Pseudo-second-order		
	$q_{e,cal}$ (mg/g)	k_2 (g/mg.min)	R^2
	73.91	8.36×10^{-3}	0.9990

Adsorption isotherms

In this study, Langmuir and Freundlich isotherm models were used to describe the adsorptive behaviour of MB dye onto CFZ NPs. Langmuir (Figure 8a) and Freundlich (Figure 8b) models parameters are listed in Table 3. As listed in the table, the correlation coefficient (R^2) value for Langmuir isotherm model (0.9906) was higher than that of Freundlich isotherm model (R^2=0.5709). This indicates the better fit of adsorption data to Langmuir isotherm model, which implies that MB dye was adsorbed as a monolayer on homogeneous surface of CFZ NPs. The maximum adsorbed amount of MB ($q_{max,}$ mg/g) was found to be 27.79 mg/g. To further evaluate the favourability of Langmuir isotherm, the separation factor (R_L) was used. The R_L values were less than unity (0.149-0.019) within the concentration range of 10 to 90 mg/L. This suggests the adsorption process of MB onto CFZ NPs is favourable [10]. Table 4. summarizes the maximum adsorbed amount (adsorption capacity) of MB using different adsorbent materials [1, 18-21, 40-42]. Based on the obtained results, the prepared magnetic nanoparticles (CFZ) are promising adsorbent materials and can be employed to treat dye-contaminated water.

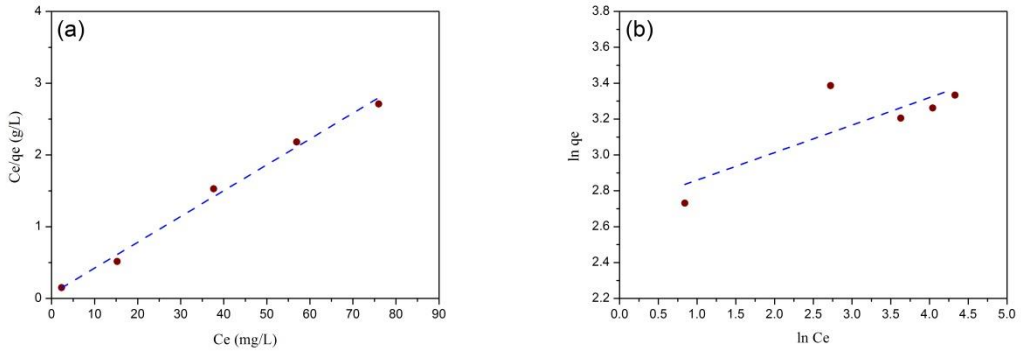

Figure 8. Isotherm plots for adsorption of MB on CFZ; (a) Langmuir isotherm model and (b) Freundlich isotherm model

Table 3. Adsorption isotherm parameters for adsorption of MB onto CFZ nanoparticles

Langmuir isotherm			Freundlich isotherm		
(q_{max} mg/g)	K_L (L/mg)	R^2	K_F (mg/g)/(mg/L)^n	n	R^2
27.79	0.571	0.9906	14.98	6.52	0.5709

Table 4. Comparison of the maximum adsorbent amount of MB onto various adsorbent materials

Adsorbent	(q_{max}, mg/g)	Reference
PANI-$NiFe_2O_4$	3.31	[21]
ZMC	4.44	[1]
CLP	6.36	[1]
$CoFe_{1.9}Cr_{0.1}O_4$	11.41	[40]
Cellulose capped Fe_3O_4	19.49	[41]
$CoFe_{1.9}Mo_{0.1}O_4$	20.45	[20]
$MnFe_2O_4$	20.7	[18]
$CoFe_{1.9}Zn_{0.1}O_4$	27.79	This study
$Mn_{0.2}Zn_{0.8}Fe_2O_4$	40.97	[42]
$NiFe_2O_4$	138.5	[19]

PANI=Polyaniline-Nickel, ZMC=Zea Mays Cobs, CLP=Citrus Limetta Peel

Adsorption Thermodynamics

The values of ΔG^o (kJ/mol) at different temperature (298, 308 and 318 K) were calculated using Equation (13). The values of ΔH^o (kJ/mol) and ΔS^o (J/mol/K) were estimated from the slope and intercept of $\ln K_c$ versus 1/T plot (Figure 9). The thermodynamic parameters are summarized in Table 5. As can be seen from the table, the values of ΔG^o were negative at all tested solution temperatures which indicate the spontaneous nature and the feasibility of the proposed adsorption process. In addition, the negative values of ΔG^o decreased with the increase in the solution temperature from 298 to 318 K. This means that the adsorption of MB onto CFZ nanoparticles is

favorable at low solution temperature. The value of ΔH^o was negative (Table 5) which indicates that the adsorption process is an exothermic in nature. Based on the ΔH^o value (−24.17 kJ/mol), it might be concluded that the adsorption of MB onto CFZ surface proceeds via physical adsorption mechanism. Furthermore, the negative value of ΔS^o indicates the decrease in the randomness at the interfacial region between the solid and liquid phases (*i.e.,* adsorbate/adsorbent interface). The obtained results are similar to those reported previously for MB adsorption using different types of adsorbents [20, 43].

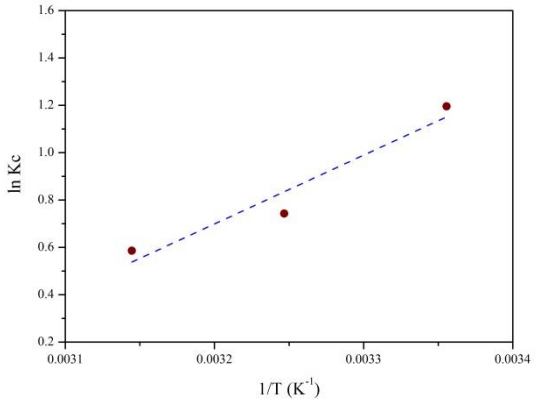

Figure 9. Adsorption thermodynamics of MB adsorption onto CFZ nanoparticles

Table 5. Thermodynamic parameters for adsorption of MB onto CFZ nanoparticles

ΔH^o (kJ/mol)	ΔS^o (J/mol.K)	ΔG^o (kJ/mol)		
		298 K	308 K	318 K
– 24.17	–71.52	– 2.86	– 2.14	– 1.43

Conclusions

In summary, a combined EDTA-citrate complexing sol-gel method was used to synthesize $CoF_{1.9}Zn_{0.1}O_4$ (CFZ) NPs. Batch mode was employed to investigate the adsorption process of MB dye onto CFZ NPs. The results demonstrated that CFZ NPs could approximately remove 77% of MB under the optimum experimental conditions (adsorbent dosage of 0.01 g/20 mL, initial pH of 7, initial dye concentration of 10 mg/L, contact time of 90 min). The adsorption kinetics followed the pseudo-second-order (PSO) kinetic model (R^2=0.9990). Langmuir isotherm (R^2=0.9906) was found to be the best model to describe the experimental data. The maximum adsorbed amount (q_{max}) of MB was about 27.79 mg of MB/g of CFZ. The adsorption thermodynamics (ΔG^o, ΔH^o, ΔS^o) revealed

that MB adsorption onto the surface of CFZ adsorbent was feasible, spontaneous, exothermic and physisorptive process.

Acknowledgement

The authors thankfully acknowledge the Department of Chemistry, Sebha University, Sebha, Libya for the financial support of this work. The authors also thank the Central Laboratory at Sebha University, Sebha Libya for providing the furnace for material calcination. The authors also thank Mr. Fathi Elsharif and Mr. Khaled Azzabi from the Nuclear Research Centre, Tajoura, Libya for performing FTIR analysis. The authors thank the Libyan Petroleum Institute, Tripoli, Libya for performing XRD and SEM analysis.

Conflict of Interest

We have no conflicts of interest to disclose.

References

[1] Singh H., Chauhan G., Jain A.K., Sharma S.K. *J. Environ. Chem. Eng*., 2017, **5**:122

[2] Rafatullah M., Sulaiman O., Hashim R., Ahmad A. *J. Hazard. Mater.*, 2010, **177**:70

[3] Ismail B., Hussain S.T., Akram S. *Chem. Eng. J.,* 2013, **219**:395

[4] Moeinpour F., Alimoradi A., Kazemi M. *J. Environ. Health Sci. Eng.,* 2014, **12**:112

[5] Kefeni K.K., Mamba B.B., Msagati T.A.M. *Separat. Purificat. Technol.*, 2017, **188**:399

[6] Santhosh C., Velmurugan V., Jacob G., Jeong S.K., Grace A.N., Bhatnagar A. *Chem. Eng. J.,* 2016, **306**:116

[7] Sun Z., Yao G., Liu M., Zheng S. *J. Taiwan Institute Chem. Eng.,* 2017, **71**:501

[8] Ahmed A., Mohd-Setapar S.H., Chuon C.S., Khatoon A., Wani W.A., Kumar R., Rafatullah M. *RSC Adv.*, 2015, **5**:30801

[9] Tan K.B., Vakili M., Horri B.A., Poh P.E., Abdullah A.Z., Salamatinia B. *Separat. Purificat. Technol.,* 2015, **150**:229

[10] Mahto T.K., Chowdhuri A.R., Sahu S.K. *J. Appl. Poly. Sci.*, 2014, **131**:40840

[11] Dawood S., Sen T.K., Phan C. *Water Air Soil Pollut.*, 2014, **225**:1818

[12] Zhang B.B., Xu J.C., Xin P.H., Han Y.B., Hong B., Jin H.X., Jin D.F., Peng X.L., Li J., Gong J., Ge H.L., Zhu Z.W., Wang X.Q. *J. Solid State Chem.*, 2015, **221**:302

[13] Zhang L., Lian J., Wang L., Jiang J., Duan Z., Zhao L. *Chem. Eng. J.*, 2014, **241**:384

[14] Kamran S., Shiri N.A. *Chem. Method.*, 2018, **2**:23

[15] Reddy D.H.K., Yun Y.S. *Coordinat. Chem. Rev.*, 2016, **315**:90

[16] Mehta D., Mazumdar S., Singh S.K. *J. Water Process Eng.,* 2015, **7**:244

[17] Gomez-Pastora J., Bringas E., Ortiz I. *Chem. Eng. J.,* 2014, **256**:187

[18] Hou X., Feng J., Ren Y., Fan Z., Zhang M. *Coll. Surfaces A: Physicochem. Eng. Aspect.,* 2010, **363**:1

[19] Hou X., Feng J., Liu X., Ren Y., Fan Z., Wei T., Meng J., Zhang M. *J. Coll. Interface Sci.*, 2011, **362**:477

[20] Amar I.A., Sharif A., Alkhayali M.M., Jabji M.A., Altohami F., AbdulQadir M.A., Ahwidi M.M. *Iranian J. Energy Environ.*, 2018, **9**:247

[21] Patil M.R., Shrivastava V. *Desalinat. Water Treat.*, 2016, **57**:5879

[22] Wang R., Yu J., Hao Q. *Chem. Eng. Res. Design*, 2018, **132**:215

[23] Ling Y., Yu J., Lin B., Zhang X., Zhao L., Liu X. *J. Power Sourc.*, 2011, **196**:2631

[24] Ahmad S.I., Ansari S.A., Kumar D.R. *Mater. Chem. Phys.,* 2018, **208**:248

[25] Kosmulski M. *Surface charging and points of zero charge*, CRC press, 2009, Chapter 1.

[26] Tran H.N., Wang Y.F., You S.J., Chao H.P. *Process Safety Environ. Protect.*, 2017, **107**:168

[27] Konicki W., Sibera D., Mijowska E., Lendzion-Bieluń Z., Narkiewicz U. *J. Coll. Interface Sci.*, 2013, **398**:152

[28] Lagergren S., *Kungliga Sevenska Vetenskapasakademiens Handlingar*, 1898, **24**:1

[29] Ho Y.S., McKay G. *Process Biochem.*, 1999, **34**:451

[30] Tran H.N., You S.J., Hosseini-Bandegharaei A., Chao H.P. *Water Res.*, 2017, **120**:88

[31] Langmuir I. *J. Am. Chem. Soc.*, 1916, **38**:2221

[32] Freundlich H.M.F. *J. Phys. Chem.*, 1906, **57**:385

[33] Bonetto L.R., Ferrarini F., Marco C.D., Crespo J.S., Guégan R., Giovanela M. *J. Water Process Eng.,* 2015, **6**:11

[34] Kumar L., Kumar P., Kar M. *J. Alloy. Compounds*, 2013, **551**:72

[35] Deb A., Kanmani M., Debnath A., Bhowmik K.L., Saha B. *Desalinat. Water Treat.*, 2017, **89**:197

[36] Zhang Y., Wu B., Xu H., Liu H., Wang M., He Y., Pan B. *NanoImpact*, 2016, **3-4**:22

[37] Al-Anber Z.A., Al-Anber M.A., Matouq M. , Al-Ayed O.O., Omari N.M.N.M. *Desalination*, 2011, **276**:169

[38] Chawla S., Uppal H., Yadav M., Bahadur N., Singh N. *Ecotoxicol. Environ. Safety*, 2017, **135**:68

[39] Mahida V.P., Patel M.P. *Arabian J. Chem.*, 2016, **9**:430

[40] Amar I.A., Sharif A., Omer N.A., Akale N.E., Altohami F.A., AbdulQadir M.A., *Synthesis and Characterization of Magnetic* $CoFe_{1.9}Cr_{0.1}O_4$ *Nanoparticles by Sol-gel Method and Their Applications as an Adsorbent for Water Treatment,* in: The First Conference for Engineering Sciences and Technology (CEST-2018) AIJR Publisher, Garaboulli, Libya, 2018, pp. 756

[41] Anushree C., Philip J. *Coll. Surfaces A*, 2019, **567**:193

[42] Hou X., Feng J., Liu X., Ren Y., Fan Z., Zhang M. *J. Coll. Interface Sci.*, 2011, **353**:524

[43] Wang P., Ma Q., Hu D., Wang L. *Desalinat. Water Treat.,* 2016, **57**:10261

How to cite this manuscript: Ibrahim A. Amar*, Abubaker Sharif, Manal Ali, Sharefa Alshareef, Fatima Altohami, Mabroukah A. AbdulQadir, Mohammed M. Ahwidi, Removal of Methylene Blue from Aqueous Solutions using Nano-Magnetic Adsorbent Based on Zinc-Doped Cobalt Ferrite. Chemical Methodologies 4(1), 2020, 01-18. DOI:10.33945/SAMI/CHEMM.2020.1.1.